M. Dębowska[1], J. Pigłowski[2], C. Ślusarczyk[3], P. Schmidt[4], J. Rudzińska- Girulska[1], T. Suzuki[5], R. Yu[5], W. Biniaś[3]

[1] **Institute of Experimental Physics, University of Wrocław,** pl. M. Borna 9, 50-524 Wrocław, Poland

[2] **Institute of Organic and Polymer Technology, Wrocław University of Technology,** Wybrzeże Wyspiańskiego 27, 50-37 Wrocław, Poland

[3] **University of Bielsko-Biała,** ul. Willowa 2, 43-309 Bielsko-Biała, Poland

[4] **Institute of Macromolecular Chemistry, Academy of Sciences of the Czech Republic,** 16206 Prague 6, Czech Republic

[5] **Radiation Science Center, High Energy Accelerator Research Organization (KEK),** Tsukuba, Ibaraki 305-0801, Japan

Is Positron Annihilation in Polyamide 6 Affected by Morphology?

Abstract

This paper presents the DSC, WAXS, SAXS, and Raman scattering measurement results, as well as the spectra the ortho-positronium mean lifetime for three PA 6 samples of different morphology. The aim of this work was estimation if the morphology of the samples influences the positron annihilation mechanism. From the ortho-positronium annihilation characteristics, it is seen that above the glass transition temperature of the unmodified PA 6, the intensity of the long-lived component depends on the packing of PA 6 chains in part of the crystalline regions in the sample. We state that only the results from the WAXS and SAXS measurements give the most detailed picture of the morphology of the investigated samples, and that the ortho-positronium characteristics seem to agree well with the WAXS and SAXS data.

Key words: *Polyamide 6, crystalline regions, positron annihilation.*

Introduction

Results of research into free volume in PA/P(n-BA-co-MMA) blends have been given in our earlier papers [1-3]. Polyamide/acrylic rubber blends exhibit a positive mixing volume accompanied by a lack of free volume additivity. The blends are not miscible. Acrylic rubber is dispersed in a glassy matrix of polyamide 6, and a good compatibility of mixture components is observed. The positive volume of mixing for the blends in the case of immiscible polymers is assumed to be evidence of looser packing of macromolecular chains and of the formation of additional free volume at the phase boundaries. The interesting question is whether the *ortho*-positronium characteristics in the positron annihilation lifetime spectra (used in the evaluation of the fractional free volume) are influenced by the presence of crystalline regions in the samples studied. Thus, the influence of crystallinity in polyamide 6 on the positron annihilation mechanism must be considered in order to properly analyse the results. In polyamide 6 two crystalline forms, α and γ (looser packing of chains), occur. In this paper, an attempt to investigate the possible influence of morphology of the polyamide 6 on the *ortho*-positronium characteristics is presented.

Sample preparation

Polyamide 6 (Stilamid S-24) was melted and homogenised in a Brabender-like mixing chamber operating at 230-240°C under nitrogen for 3 min. Immediately after melting, the melted mass was placed in a hot press, and 2-mm thick plates were moulded. The plates were cut into strips (denoted as PA6 raw). Some strips were additionally modified in two ways: a) PA strips were melted once more and then quenched in liquid nitrogen (PA6 LN), b) they were treated with water vapour in a Melag autoclave (134 °C, 2.1 bar, 3 cycles each 30 min, denoted as PA6 H_2O).

Results

DSC measurements

Differential scanning calorimetry (DSC) measurements were carried out on a Mettler Toledo DSC 821 apparatus. All the samples were first melted (25-245°C, heating rate 10 K/min), held for 2 min at 245°C to destroy all the crystallites, and then cooled to -30°C at a cooling rate of -10K/min, maintained for 1 minute at this temperature, and again heated to 245°C with a heating rate of 10 K/min. Values of melting enthalpies (ΔH_m) were obtained from the area of endothermic peaks. The crystallinity degrees were calculated according to the following equation:

$$X_{cr} = \frac{\Delta H_m}{\Delta H_{100}} \qquad (1)$$

where ΔH_m is the measured value of the melting enthalpy and ΔH_{100} is the enthalpy of 100% crystalline PA taken as 190 J/g [4].

As the polyamide samples were exposed to different thermal and chemical treatment, the first scan upon heating is of particular interest. It is interesting to compare the DSC traces from the first and second scans upon heating, since they can reflect the structural changes caused by different processing conditions. The heating curves (1st scan) for the PA samples

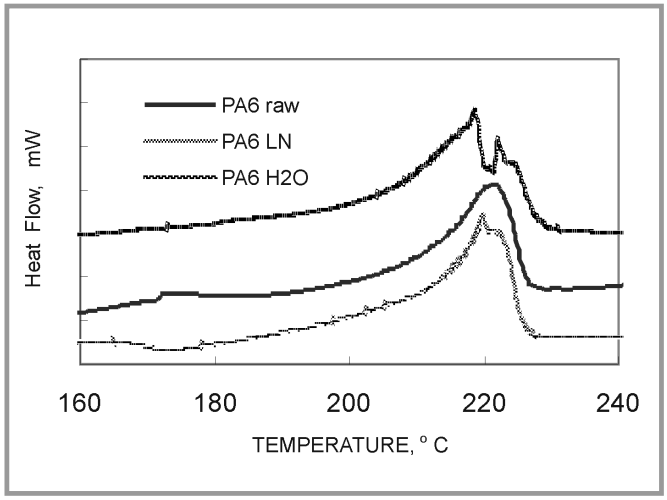

Figure 1. *Melting behaviour during the first scan (from the top to bottom: PA6 raw, PA6 LN and PA6 H_2O).*

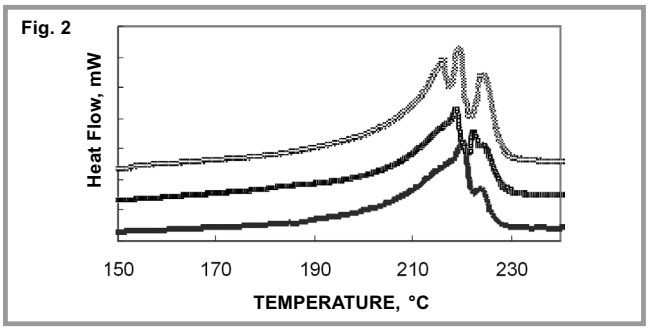

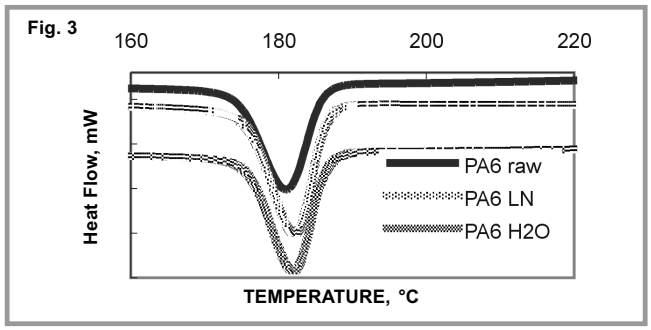

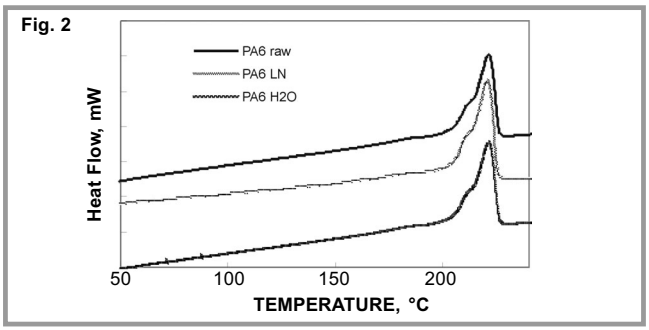

Figure 2. *Examples of melting behaviour of PA6 H_2O samples processed in the autoclave.*

Figure 3. *Crystallisation exothermic curves for PA6 raw, PA6 LN and PA6 H_2O (from the top to bottom).*

Figure 4. *Melting behaviour during the second scan (from top to bottom: PA6 raw, PA6 LN and PA6 H_2O).*

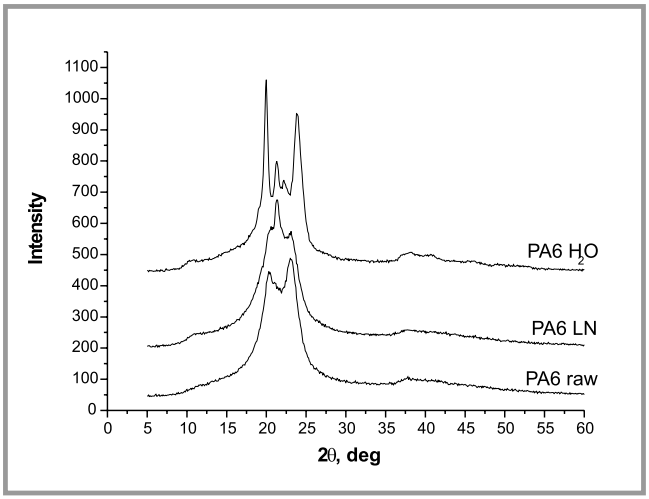

Figure 5. *Comparison of WAXS curves for PA6 raw, PA6 LN and PA6 H_2O. Curves have been shifted along the Y axis for better clarity.*

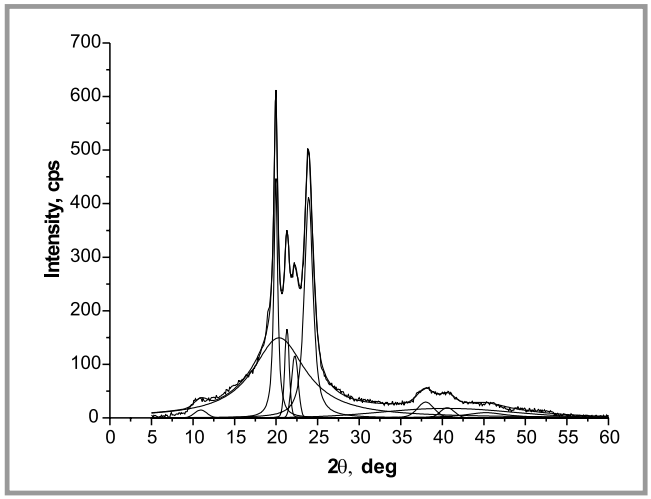

Figure 6. *WAXS pattern of the sample PA6 H_2O – amorphous and crystalline components.*

are shown in Figure1. Polyamide 6 as received (PA6 raw) and quenched polyamide (PA6 LN) show nearly the same melting peaks. A small exothermal peak just before the melting point of PA6 LN indicates the so-called pre-melt crystallisation. This is evidence that this sample has not reached its maximum crystallinity.

In spite of this, the crystallinity level of PA6 LN is only somewhat smaller than in PA6 raw (Table 1). The structure of polyamide 6 crystallised from the melt may be influenced by several factors such as thermal history, applied stress, moisture and the additives that are present. In general, rapid cooling and a low crystallisation temperature promotes the γ-form of polyamide 6, while higher crystallisation temperatures or a slow cooling rate lead to the a-form. Our results do not indicate polymorphism; only monoclinic crystallites melt at 220-222°C are visible, there is no hexagonal fraction at 215°C. Completely different melting behaviour was observed for the polyamide processed in an autoclave under high pressure, water vapour and temperature (PA6 H_2O). Here the main endothermic peak, related to the a-form, splits up. Both phases probably have the same chain arrangement characteristic of the monoclinic form, but the higher peak corresponds to crystallites with bigger lamellar thickness. Additionally, the formation of a small shoulder prior to the maximum of the endothermic peak is visible. It may be associated with the γ

Table1. *Melting enthalpies, melting temperatures and level of crystallinity for PA samples.*

Sample	1st scan			2nd scan		
	ΔH (J/g)	T_m(°C)	crystallinity (wt.-%)	ΔH (J/g)	T_m(°C)	crystallinity (wt.-%)
PA6 raw	67.12	222	35	56.02	221	29
PA6 LN	63.44	220	33	56.35	221	29
PA6 H_2O	88.29	219 223	46	55.40	221	29

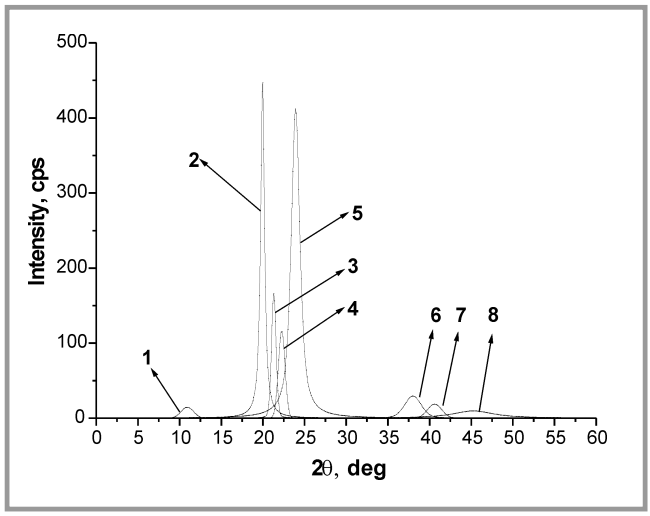

Figure 7. *WAXS pattern of the sample PA6 H_2O – combination of the crystalline components: 1 – α (002), 2 – α (200), 3 – γ (200), 4 – γ (020), 5 – α (020/220), 6 – α (2-20/420), 7 – γ (004), 8 – α (-240).*

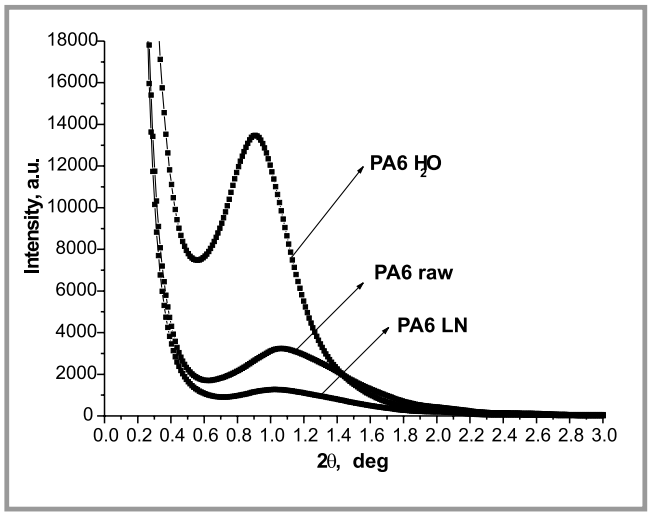

Figure 8. *Comparison of SAXS patterns for the studied samples. The scattering indicates the existence of a superstructure with periodic fluctuations of elelctron densities.*

crystalline form of polyamide 6, as suggested by various research works [5, 6].

Most experiments with PA6H_2O show a double peak with small shoulder at low temperature during the first melting (see examples of two traces in the upper part of Figure 2). Nevertheless, for this sample one can find DSC traces with the third peak also. The third endotherm maximum, located at 115°C, is associated with the presence of γ crystallites in the PA6 H_2O. Such discrepancies during the first melting may be caused by irregular heat transfer depending on the shape of the sample when processed in the autoclave.

The results of non-isothermal crystallisation studies are presented in Figure 3. All samples exhibit nearly the same crystallisation temperature and peak width regardless of their prior thermal history. Stress and thermal histories do not remain after melting.

After the same crystallisation conditions (not only in terms of experimental parameters), all three samples, i.e. PA6 raw, PA6 LN and PA6 H_2O, show identical behaviour during the second melting scan (Figure 4). The corresponding melting peaks at 221°C exhibit shoulders at 210°C that are associated with a small amount of the polyamide γ-form.

X-ray measurements

Wide-angle X-ray diffraction (WAXS) investigations were conducted at room temperature using a Seifert URD-6 diffractometer in the reflection mode using Ni-filtered CuK_α radiation. The diffraction scans were collected between 2θ values from 5° to 60° with a step of 0.1°.

Polyamide 6 is a polymer with two crystalline modifications, namely α phase and γ phase. The α phase has a monoclinic structure, where neighbouring anti-parallel chains form hydrogen bonds, which in turn generate a planar hydrogen-bonded sheet (ac-plane). These sheets stack together via van der Waals interactions. This structure gives two inter-chain diffraction signals at spacings of 0.44 nm (indexed as (200)) and 0.37 nm (indexed as (020)/(220)), respectively. The single sheet generates a (002) diffraction signal from the planes of C=O groups at a spacing of 0.862 nm (see Figure 7).

The γ modification also has a monoclinic structure, but because the amide units tilt and rotate out of the ac-plane, hydrogen bonds occur between parallel chains, which explains a reduction of the two inter-chain distances in the region of 0.40 – 0.42 nm. The hydrogen bonding is poorer in the ă-form compared to the γ-form.

The WAXS data shown in Figure 5 revealed that α and γ forms co-exist in all the samples studied. Which one of them is predominant depends on the sample preparation conditions: the time and temperature of crystallisation, or the presence of moisture or certain additives. In order to determine the content of these polymorphic forms, the WAXS curves were deconvoluted into crystalline and amorphous scattering components using the OptiFit profile fitting program [7]. Each peak was modelled using a Gaussian-Cauchy peak shape. The areas of the peaks obtained from the analysis were used to estimate the degree of crystallinity for each phase, i.e. the ratio of the areas of the crystalline reflections to that of the total area of the scattering curve (amorphous + crystalline). Figure 6 is a representative example of a diffraction curve that has been resolved into crystalline and amorphous scattering components using the peak fitting software. Moreover, the crystalline peaks are presented in the separate Figure 7 for better visualization.

WAXS measurements indicate that the best crystalline structure appears in the sample PA6 H_2O. Respective peaks are clearly separated. The reflections corresponding to α(002) and γ(004) – weak or not detectable in case of other samples – are clearly visible here. Rapid cooling in liquid nitrogen resulted in the highest content of the ă- form (less stable in a thermodynamic sense and less dense) in the PA6 LN sample. The studied samples differ in the size of the crystalline regions. The largest crystallites are present in the sample PA6 H_2O.

The small-angle X-ray (SAXS) investigations were performed by means of a MBraun (Austria) SWAX camera which utilises the conventional Kratky collimation system. The front of the camera was directly mounted on the top of the tube shield of a stabilised Philips PW 1830 X-ray generator. The X-ray tube worked at a power of. 1.5 kW. CuK_α; monochromatisation was performed by a Niβ filter

and pulse height discrimination. The entrance slit was adjusted to 50 μm. Scattered radiation was recorded over a counting time of 900 s by means of an MBraun linear position-sensitive detector, PSD 50 model. The detector had 1024 channels with a channel-to-channel distance of 52 μm. The experimental SAXS curves were corrected for sample absorption and desmeared of collimation distortions by means of the 3DVIEW computer program supplied by MBraun.

SAXS patterns for studied samples are shown in Figure 8. The appearance of the scattering peak indicates the existence of a superstructure with periodic fluctuations of electron densities, which are mainly related to the alternating lamellar and amorphous layers. Further analysis of SAXS data was carried out by means of the correlation function which allows the lamellar thickness (l_c) and the amorphous layer thickness (l_a) to be determined, as well as the long period $L = l_c + l_a$. The results are presented in Table 2. The best lamellar structure appears in case of the sample PA6 H_2O, in which the thickness of the amorphous layer is the highest (c.f. the values of the long period from the correlation function-L and thickness of the crystalline lamellae-l_c given in Table 2). SAXS results indicate that the lamellar morphology is the most uniform in the PA6 H_2O sample. The DSC (first scan) detected the γ-form only for the PA6 H_2O sample.

Raman scattering

The Raman spectra were acquired using the Magna System 860 spectrometer. A laser power of 1.5 W and a resolution of 8 cm^{-1} were used. The diameter of the laser beam was 0.25 mm. Five different regions of each sample were studied. Then, the results of the measurements were summarised and averaged.

The Raman spectra were analysed (Figure 9) in the way described in [8, 9]. The band 1125 cm^{-1}, characteristic of the planar A conformation (present only in the α-crystalline form), and the band 1079 cm^{-1}, characteristic of the twisted B conformation (present in the mesomorphous material and the γ-crystalline form) were taken into account. The intensity ratio of the bands (I_{1079}/I_{1125}) higher than 1 for PA6 raw and PA6 LN corresponds well to the WAXS data for the samples. On the other hand, rough estimation indicates that more than 50% of the α-crystalline form is present in the sample PA6 H_2O, which does not coincide with the WAXS data. The total crystallinity of the sample from DSC is 46%.

Positron lifetime measurements

Positrons are well established probes of electronic structure, surface, defects and phase transitions (for further details see [10]). Positron annihilation in polymers have been the focus of attention for investigators from the very beginning of the development of positron annihilation spectroscopy [11]. Long lifetimes (of the order of 10^{-9} s) occurring in positron annihilation lifetime spectra, measured for polymer samples, result from the pick-off annihilation of *ortho*-positronium. Positronium (the bound state of a positron and an electron), due to its interaction with a medium, localises in regions of low density existing in a substance: pores in porous materials, free volume holes in polymers, or even those which it creates (c.f. bubbles in liquids).

According to a simple quantum-mechanical model [12, 13], the *ortho*-positronium lifetime and its intensity extracted from the lifetime spectra give the information on the region where the *ortho*-positronium (o-Ps) was annihilated.
Such a trap is approximated by a well of an infinite square potential of spherical symmetry (for further details see [14]). The pick-off annihilation of the *ortho*-positronium takes place with electrons from a layer with constant density of electronic charge and width ΔR. The o-Ps lifetime τ in that case is given as follows:

$$\tau = 2^{-1}\left[1 - \frac{R}{R+\Delta R} + (2\pi)^{-1}\sin\left(\frac{2\pi R}{R+\Delta R}\right)\right]^{-1} \quad (2)$$

where *R* denotes the radius of the spherical trap, while ΔR=1.656 Å for molecular solids. This is an empirical parameter obtained by fitting the measured o-Ps lifetimes in materials of well-defined empty space (e. g. pores in zeolites [15].

Positron annihilation lifetime spectra were measured using a conventional fast-fast coincidence system with a gaussian function of the time resolution with FWHM of about 270ps. The channel width was 40 ps/channel. The sample chamber was pumped by a vacuum system (up to 10^{-7} mmHg), and combined with a cooling system (CW303, Iwatani) with a temperature control device for automatic measurement from 35 to 370 K at a 5 K/h rate. The positron annihilation lifetime spectrum was saved every hour, resulting in about 1.2 million events in each spectrum. The experimental spectra were analysed using the LIFETIME programme v. 9 [16]. Two discrete short-lived components with lifetimes of $\tau_1 \approx$

Table 2. *Results of WAXS and SAXS Studies.*

Sample	Crystallinity (wt.%)	Weight fraction of α form	Weight fraction of γ form	$D_{\alpha(200)}$ [nm]	$D_{\gamma(200)}$ [nm]	L [nm]	l_c [nm]
PA6 raw	0,461	0,387	0,074	3,3	3,7	6,3	2,9
PA6 LN	0,462	0,348	0,114	2,7	5,4	6,2	2,5
PA6 H_2O	0,441	0,363	0,078	10,7	12,1	8,4	3,2

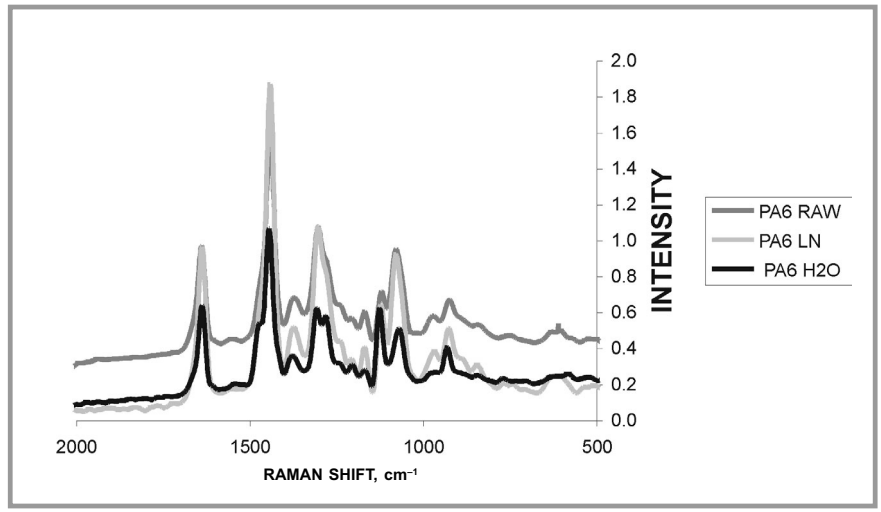

Figure 9. *The Raman spectra for the studied samples.*

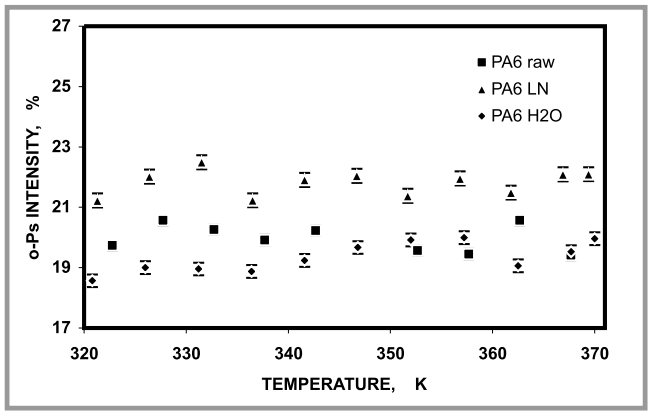

Figure 10. *The intensity of the long-lived component in the positron annihilation lifetime spectra.*

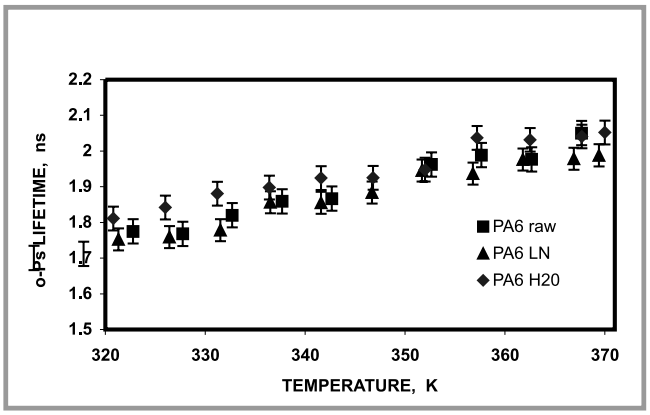

Figure 11. *The mean lifetime of the log-normal distribution of* ortho-*positronium lifetimes.*

140 ps and $\tau_2 \approx 400$ ps, and one long-lived one with log-normal distributions of the lifetimes appeared to fit the experimental spectra best. It is generally assumed that the long-lived component comes from the *ortho*-positronium annihilation by pick-off in free volume holes. The intensity and the mean value of the log-normal distribution of the lifetimes are used for characterising free volume in polymers. The intensity and the mean value of the log-normal distribution of lifetimes corresponding to the long-lived component are given for the samples studied in Figures 10 and 11.

Conclusions

- Changes in crystallinity and morphology of the polyamide due to special treatment with water vapour and liquid nitrogen (although not so great as expected) were detected by all methods (DSC, X-ray diffraction and Raman scattering).

- The values of total crystallinity from X-ray diffraction are higher than the corresponding ones from DSC in the cases of PA6 raw and PA6 LN, while in the case of PA6 H_2O, the sample of the best crystalline structure, the results of the two methods are very close. The total crystallinity was not estimated from Raman scattering.

- The information on morphology of samples obtained from X-ray diffraction is not supported by the DSC results (no polymorphism of the PA6 raw sample and the PA6 LN), while rough estimation of the α- form content in PA6 raw and PA6 LN from Raman scattering (~35%) is in good agreement with the estimation from the WAXS data. However, the α-form content in PA6 H_2O was overestimated on the basis of data from the Raman scattering.

- From the *ortho*-positronium annihilation characteristics, it is seen that above the glass transition temperature of the unmodified PA6, the intensity of the long-lived component is distinctly higher for the sample PA6 LN than for the PA6 raw and PA6 H_2O samples. This may be connected with the looser packing of PA6 chains in part of the crystalline regions in the sample. The results of WAXS indicate that in PA6 LN the content of the γ-form is higher than in the samples of PA6 raw and PA6 H_2O. Taking into account that the density of γ phase is about 6% less than the density of α phase, these subtle changes in the γ phase content can affect the long-lived component.

- In Figure 11, in the same region of temperature as the above points corresponding to the mean lifetime of the *ortho*-positronium in PA6 H_2O are arranged a little higher in comparison to those for PA6 raw and Pa6 LN. One may suspect that it is the result of the influence of the better crystalline structure on the neighbouring amorphous regions. Stretching those regions could result in broadening the amorphous layer as seen from the SAXS data and increase in size of the free volume holes. As an indication of the latter, one could assume the tendency of the arrangement of the points for the PA6 H_2O sample seen in Figure 11.

- At this stage of our studies, only the results from the WAXS and SAXS measurements give the most detailed picture of the morphology of the investigated samples. The *ortho*-positronium characteristics, extracted from the positron annihilation lifetime spectra, seem to agree well with the WAXS and SAXS data.

❑

References

1. *M. Dębowska, J. Rudzińska-Girulska, J. Pigłowski, T. Suzuki, Cz. Ślusarczyk, Fibres and Textiles in Eastern Europe,* ***11****, No. 5(44), 120 (2003).*
2. *M. Dębowska, J. Pigłowski, J. Rudzińska-Girulska, T. Suzuki, Z. Q. Chen, Radiation Physics and Chemistry,* ***68****, 471 (2003).*
3. *M. Dębowska, J. Pigłowski, T. Suzuki, J. Rudzińska-Girulska, Cz. Ślusarczyk and W. Biniaś, Materials Science Forum,* ***445-446****, 277 (2004).*
4. *J.Brandrup, E. Immergut, Polymer Handbook, (1989), 3rd ed. New York, Wiley.*
5. *I. Campoy, M. A. Gomez, C. Marco, Polymer,* ***39****(25), 6279 (1998).*
6. *T. M. Wu, E. C. Chen, C. S. Liao, Polym.Eng.Sci.,* ***42****(6), 1141 (2002).*
7. *M. Rabiej, Fibres and Textiles in Eastern Europe,* ***11****, No. 5(44), 83 (2003).*
8. *P. Schmidt, P. J. Hendra, Spectrochimica Acta, (1994),* ***50A****(11),1999.*
9. *P. Schmidt, M. R. Fernandez, J. M. Pastor, J. Roda, Polymer, (1997),* ***38****(9), 2067.*
10. *'Positrons in Solids", ed. P. Hautojärvi, Springer-Verlag, Berlin, 1979.*
11. *S. De Benedetti, H. J. Richings, Phys. Rev.* ***85****, 377 (1952); R. E, Bell, R. L. Graham, Phys. Rev.* ***90****, 644 (1953).*
12. *S. J. Tao, J. Chem. Phys.* ***56****, 5499 (1972).*
13. *M. Eldrup, D. Lightbody, J. N. Sherwood, Chem. Phys.* ***63****, 51 (1981).*
14. *H. Nakanishi and Y. C. Jean in: 'Positron and Positronium Chemistry', eds. D. M. Schrader and Y. C. Jean, Elsevier, Amsterdam, 1988, p. 168.*
15. *H. Nakanishi, S. J. Wang, Y. C. Jean in: 'Positron Annihilation Studies of Fluids', ed. S. C. Sharma, World Scientific, Singapore, 1988, p. 292.*
16. *J. Kansy in: Proceedings of the 34th Polish Seminar on Positron Annihilation (Turawa, Poland, June 16-21, 2002), ed. By K. Jerie, Institute of Physics (University Opole), Institute of Experimental Physics (University of Wrocław), p. 179, Opole 2002; J. Kansy, Nuclear Instruments and Methods in Physics Research, A 10555, 1 (1996).*

❑ ***Received 08.12.2004 Reviewed 10.02.2005***